AD-A102 258 OHIO STATE UNIV COLUMBUS ELECTROSCIENCE LAB F/G 20/14
THE EFFECT OF A PULSED INTERFERENCE SIGNAL ON AN ADAPTIVE ARRAY--ETC(U)
APR 81 R T COMPTON N00019-80-C-0181
UNCLASSIFIED ESL-712684-8 NL

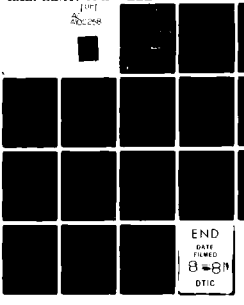

LEVEL II

12

OSU

The Ohio State University

THE EFFECT OF A PULSED INTERFERENCE SIGNAL ON AN ADAPTIVE ARRAY

R.T. Compton, Jr.

AD A102258

The Ohio State University

ElectroScience Laboratory

Department of Electrical Engineering
Columbus, Ohio 43212

Technical Report 712684-8
Contract N00019-80-C-0181
April 1981

Department of the Navy
Naval Air Systems Command
Washington, D.C. 20361

NOTICES

When Government drawings, specifications, or other data are used for any purpose other than in connection with a definitely related Government procurement operation, the United States Government thereby incurs no responsibility nor any obligation whatsoever, and the fact that the Government may have formulated, furnished, or in any way supplied the said drawings, specifications, or other data, is not to be regarded by implication or otherwise as in any manner licensing the holder or any other person or corporation, or conveying any rights or permission to manufacture, use, or sell any patented invention that may in any way be related thereto.

Unclassified

SECURITY CLASSIFICATION OF THIS PAGE (When Data Entered)

REPORT DOCUMENTATION PAGE	READ INSTRUCTIONS BEFORE COMPLETING FORM
1. REPORT NUMBER	2. GOVT ACCESSION N AD-A102 258 / 3. RECIPIENT'S CATALOG NUMBER
4. TITLE (and Subtitle) (6) THE EFFECT OF A PULSED INTERFERENCE SIGNAL ON AN ADAPTIVE ARRAY.	5. TYPE OF REPORT & PERIOD COVERED (9) Technical Report.
	6. PERFORMING ORG. REPORT NUMBER (14) ESL-712684-8
7. AUTHOR(s) (10) R.T. Compton, Jr.	8. CONTRACT OR GRANT NUMBER(s) (15) Contract N00019-80-C-0181
9. PERFORMING ORGANIZATION NAME AND ADDRESS The Ohio State University ElectroScience Laboratory, Department of Electrical Engineering Columbus, Ohio 43212	10. PROGRAM ELEMENT, PROJECT, TASK AREA & WORK UNIT NUMBERS
11. CONTROLLING OFFICE NAME AND ADDRESS (11) Department of the Navy Naval Air Systems Command Washington, D.C. 20361	12. REPORT DATE April 1981 (12) 43 / 13. NUMBER OF PAGES 37
14. MONITORING AGENCY NAME & ADDRESS (if different from Controlling Office)	15. SECURITY CLASS. (of this report) Unclassified / 15a. DECLASSIFICATION/DOWNGRADING SCHEDULE
16. DISTRIBUTION STATEMENT (of this Report) Approved for public release; distribution unlimited	
17. DISTRIBUTION STATEMENT (of the abstract entered in Block 20, if different from Report)	
18. SUPPLEMENTARY NOTES	
19. KEY WORDS (Continue on reverse side if necessary and identify by block number)	

20. ABSTRACT (Continue on reverse side if necessary and identify by block number)

This report examines the performance of an LMS adaptive array in the presence of a pulsed interference signal. It is shown that a pulsed interference signal has two effects. First, it causes the array to modulate the desired signal envelope (but not its phase). Second, it causes the array output signal-to-interference-plus-noise ratio (SINR) to vary with time. The desired signal modulation is evaluated as a function of signal arrival angles, powers and interference PRF and pulse width. It is shown that the signal modulation is small except when the interference arrives close to the desired signal. To evaluate the effect of →

DD FORM 1 JAN 73 1473 EDITION OF 1 NOV 65 IS OBSOLETE

Unclassified

SECURITY CLASSIFICATION OF THIS PAGE (When Data Entered)

the time-varying SINR, it is assumed that the array is used in a DPSK communication system. It is shown that the SINR variation causes a noticeable but not disastrous increase in the bit error probability.

I. INTRODUCTION

Adaptive arrays based on the LMS algorithm of Widrow, et al [1] are very useful for protecting communication systems from interference [2,5]. These antennas can automatically null interference signals from arbitrary arrival angles, with arbitrary polarizations[6,7], and of arbitrary power.*

A subject that has received little attention in the literature, however, is the performance of these arrays with modulated interference. Most studies on adaptive array performance have assumed interference signals with constant power. An interference signal whose power varies with time, however, may be more difficult for the array to null. If the modulation rate of the interference is close to the natural response rate of the array, such a signal may keep the array in a perpetual transient state.

In this paper, we examine the performance of an LMS array with such a signal, a pulsed interference signal. Pulsed interference is perhaps the simplest type of modulated signal to study, because at any given time the interference is either on or off. Pulsed interference causes the array weights to alternate between two sets of values. When the pulse is on, the weights move toward values that null the interference. When the pulse is off, the weights relax back toward the values they would have without interference. If the pulse width or the time between pulses is close to the weight time constants, the array weights may never reach steady-state. If the array does not form a steady-state null, the output interference power is higher during the pulse than it would be if the interference were continuous.

As we will show, pulsed interference has two effects on array performance. First, it causes the array to modulate the desired signal. Second, it causes the output signal-to-interference-plus-noise ratio (SINR) to vary with time. In this paper we relate these effects to the interference pulse width, repetition frequency, power and arrival angle, as well as to the desired signal power and arrival angle.

In spite of the fact that pulsed interference appears more dif-

---

*Within the dynamic range of the circuitry.

ficult for an adaptive array to null, we shall show that in fact such interference is not a major problem for the array. First, we find that the envelope modulation is small unless the interference arrival angle is very close to that of the desired signal. (In this case, continuous interference is also a problem!) Second, we show that although pulsed interference does reduce system SINR, the degradation is not disastrous. (To evaluate this effect meaningfully, we assume the array is used in a digital communication system and compute the effect of the SINR change on bit error probability.)

In Section II of the paper, we define the array and the signals, and formulate the necessary equations. Section III contains the results.

II. FORMULATION

Consider the 3-element adaptive array shown in Figure 1. The elements are assumed isotropic, noninteracting and a half wavelength apart at the signal frequency. The analytic signal $\tilde{x}_j(t)$ received on element j is multiplied by a complex weight w_j and summed to produce the array output $\tilde{s}(t)$. The signals from the 3 elements are combined with an LMS processor [1], for which the weights satisfy the system of equations

$$\frac{dW}{dt} + k\Phi W = kS \quad , \tag{1}$$

where k is the LMS loop gain, $W = (w_1, w_2, w_3)^T$ is the weight vector, Φ is the covariance matrix,

$$\Phi = E\,(X^* X^T), \tag{2}$$

and S is the reference correlation vector,

$$S = E\,(X^* \tilde{r}(t)). \tag{3}$$

Here X is the signal vector $X = (\tilde{x}_1(t), \tilde{x}_2(t), \tilde{x}_3(t))^T$, and $\tilde{r}(t)$ is the reference signal [3]. Also, E (·) denotes expectation, * complex conjugate and T transpose.

We assume a desired signal and a pulsed interference signal are incident on the array, and also assume thermal noise is present in each element signal. The signal vector X then contains three terms,

$$X = X_d + X_i + X_n, \tag{4}$$

where X_d, X_i and X_n are the desired, interference and thermal noise vectors, respectively. These vectors are defined as follows.

First, we assume the desired signal is a CW signal incident from angle θ_d relative to broadside. (θ is defined in Figure 1.) The desired signal vector is then

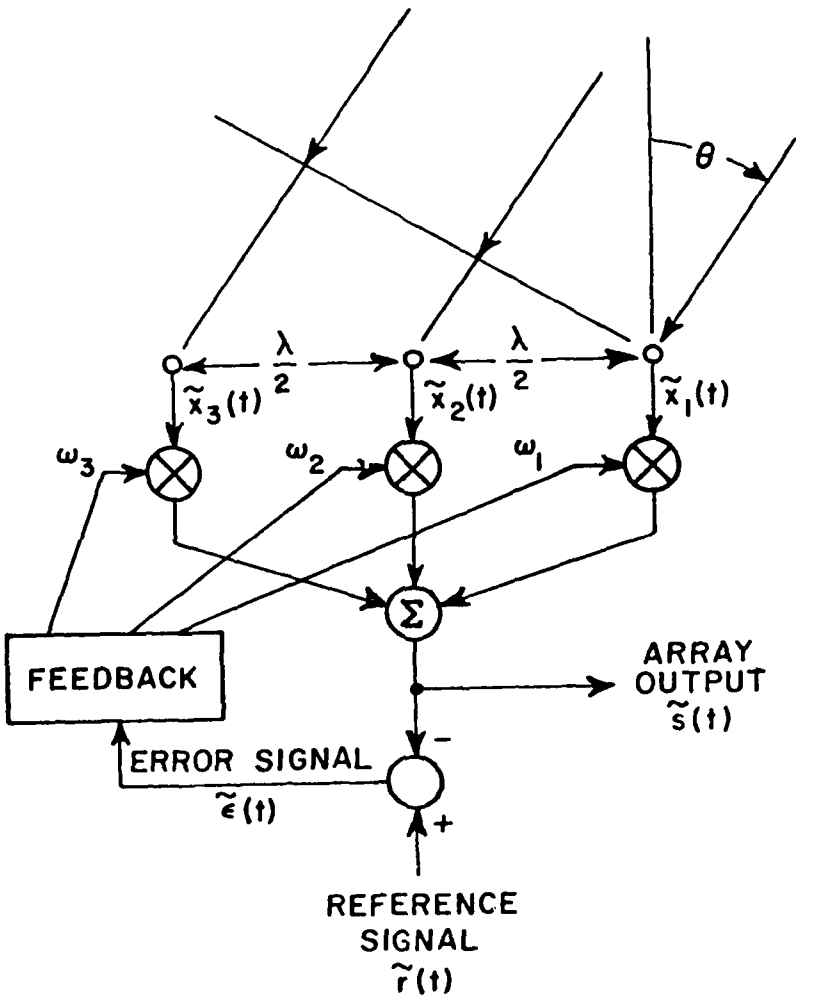

Figure 1. A 3-Element Adaptive Array

$$X_d = A_d e^{j(\omega_o t + \psi_d)} U_d \ , \tag{5}$$

where A_d is the amplitude, ω_o the carrier frequency, and ψ_d the carrier phase angle. U_d is a vector containing the interelement phase shifts,

$$U_d = (1, e^{-j\phi_d}, e^{-j2\phi_d})^T \tag{6}$$

with

$$\phi_d = \pi \sin \Theta_d. \tag{7}$$

We assume ψ_d is a random variable uniformly distributed on $(0, 2\pi)$.

Next, we assume the interference is a pulse modulated carrier, as shown in Figure 2, arriving from angle Θ_i. We let τ be the pulse width and T_r the pulse repetition period. The pulse repetition frequency (PRF) is then $f_r = 1/T_r$ and the duty cycle is $\delta = \tau/T_r$. The interference signal vector is

$$X_i = a_i(t) e^{j(\omega_o t + \psi_i)} U_i \ , \tag{8}$$

where $a_i(t)$ is the envelope modulation, ψ_i the carrier phase, and

$$U_i = (1, e^{-j\phi_i}, e^{-j2\phi_i})^T, \tag{9}$$

with

$$\phi_i = \pi \sin \Theta_i. \tag{10}$$

The modulation $a_i(t)$ is given by

$$a_i(t) = \begin{cases} A_i : nTr \leq t \leq nTr + \tau \\ 0 : nTr + \tau < t < (n+1)\,Tr \end{cases}, \tag{11}$$

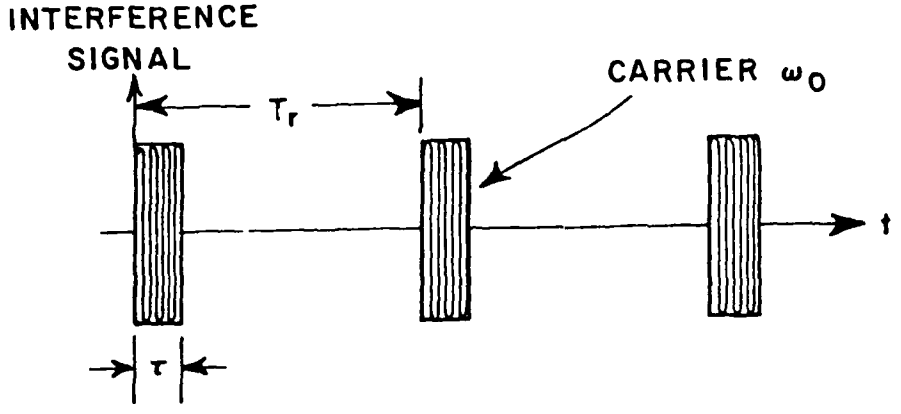

Figure 2. The Pulsed Interference Signal

where n is an integer denoting the period and A_i is the pulse amplitude. Thus, X_i is equal to $A_i e^{j(\omega_o t + \psi_i)} U_i$ when the pulse is on and is zero when it is off. We assume ψ_i is uniformly distributed on $(0, 2\pi)$ and statistically independent of ψ_d.

Finally, the thermal noise vector is

$$X_n = (\tilde{n}_1(t), \tilde{n}_2(t), \tilde{n}_3(t))^T, \tag{12}$$

where the $\tilde{n}_j(t)$ are zero-mean, gaussian thermal noise voltages. We assume each $\tilde{n}_j(t)$ is statistically independent of the others and has variance σ^2:

$$E[\tilde{n}_j^*(t)\tilde{n}_k(t)] = \sigma^2 \delta_{jk}, \tag{13}$$

where δ_{jk} is the Kronecker delta. Also, we assume the $\tilde{n}_j(t)$ are statistically independent of ψ_d and ψ_i.

From X_d, X_i and X_n, one finds that the covariance matrix in (2) has one of two forms, depending on whether the pulse is on or off. When the interference is on (for $nT_r \leq t \leq nT_r + \tau$),

$$\Phi = \Phi_p = \sigma^2 I + A_d^2 U_d^* U_d^T + A_i^2 U_i^* U_i^T, \tag{14}$$

and when the interference is off (for $nT_r + \tau < t < (n+1)T_r$),

$$\Phi = \Phi_o = \sigma^2 I + A_d^2 U_d^* U_d^T, \tag{15}$$

where I is the identity matrix. The pulse modulation causes Φ to switch back and forth between these two forms.

To compute the reference correlation vector S, the reference signal must also be defined. Let $\tilde{r}(t)$ be a CW signal of amplitude A_r coherent with the desired signal,*

$$\tilde{r}(t) = A_r e^{j(\omega_o t + \psi_d)}. \tag{16}$$

Then since X_i and X_n are uncorrelated with $\tilde{r}(t)$, (3) yields

$$S = A_r A_d U_d^*. \tag{17}$$

Now consider what happens with pulsed interference. In general, for a given Φ and S, the transient solution to (1) has the form **

$$W(t) = e^{-k\Phi t}\,[W(0) - \Phi^{-1}S] + \Phi^{-1}S, \tag{18}$$

---

*In practice, $\tilde{r}(t)$ does not need to be identical to the desired signal, but it must be correlated with the desired signal and uncorrelated with the interference. Methods of obtaining reference signals in practical communication systems have been described in [3-5].

**Matrix exponentials such as $e^{-k\Phi t}$ are discussed in [8,9].

where W(t) is the weight vector at time t and W(0) is its initial value at t=0. W(t) varies exponentially from W(0) at t=0 to its final value $\Phi^{-1}S$ at $t=\infty$. Suppose the weights are initially in steady-state with the array receiving desired signal but no interference (i.e., $W(0)=\Phi_o^{-1}S$). Also, suppose the first interference pulse arrives at t=0. At this instant, the covariance matrix changes from Φ_o to Φ_p. The weight vector begins an exponential transient starting from $\Phi_o^{-1}S$ and going to $\Phi_p^{-1}S$. If the pulse length τ is long compared to the duration of the transient, the weight vector will reach the new steady-state value $\Phi_p^{-1}S$. But if τ is too short, the transient will not be finished when the pulse ends. In either case, at $t=\tau$ the interference disappears. The covariance matrix again becomes Φ_o, and the weight vector begins a second transient returning to $\Phi_o^{-1}S$. Depending on the time duration $T_r-\tau$ when the pulse is off, the weight vector may or may not finish this second transient before the next pulse occurs.

In general, when pulsed interference first appears, the weight vector is a nonperiodic function during the first few pulse repetition periods. After an initial interval, however, the weight vector settles into a periodic behavior. The duration of the initial interval depends on the array time constants and on the initial weight vector (as will be discussed below.) If either τ or $T_r-\tau$ are long compared to the duration of the weight transients in their respective intervals, the weight vector will reach steady-state during one of both of these intervals. In this case, the weight vector will essentially be periodic from the first pulse on. However, if both τ and $T_r-\tau$ are too short for the transients to finish during either interval, the weights will not have completed one transient before the next one begins. Several cycles of the pulse repetition period will then be required for the weight vector to become periodic. After an initial interval, however, the weight vector always becomes periodic.

Before examining the initial transient behavior in detail, we first consider the periodic case. Suppose a typical period of the interference begins at t=0. Let the weight vector at t=0 be W_1. During the interval $0 \leq t \leq \tau$, the weight vector is given by

$$W(t) = e^{-k\Phi_p t}[W_1 - \Phi_p^{-1}S] + \Phi_p^{-1}S. \tag{19}$$

Let the value of W(t) at the end of the pulse (at $t=\tau$) be W_2:

$$W_2 = e^{-k\Phi_p \tau}[W_1 - \Phi_p^{-1}S] + \Phi_p^{-1}S. \tag{20}$$

W_2 is then the initial value for the weight transient that occurs during the interval when the pulse is off. Hence, for $\tau \leq t \leq T_r$,

$$W(t) = e^{-k\Phi_o(t-\tau)}[W_2 - \Phi_o^{-1}S] + \Phi_o^{-1}S. \tag{21}$$

Since W(t) is periodic by assumption, at $t=T_r$ W(t) will have returned to its initial value W_1. Thus

$$W_1 = e^{-k\Phi_o(T_r-\tau)}[W_2 - \Phi_o^{-1}S] + \Phi_o^{-1}S. \tag{22}$$

Combining (20) and (22) allows us to solve for the two unknown weight vectors W_1 and W_2. (20) and (22) together yield the system of equations

$$\left(\begin{array}{c|c} -e^{-k\Phi_p\tau} & I \\ \hline I & -e^{-k\Phi_o(T_r-\tau)} \end{array}\right)\left(\begin{array}{c} W_1 \\ \hline W_2 \end{array}\right) = \left(\begin{array}{c} [I - e^{-k\Phi_o(T_r-\tau)}]\Phi_o^{-1}S \\ \hline [I - e^{-k\Phi_p\tau}]\Phi_p^{-1}S \end{array}\right), \tag{23}$$

where we use a partitioned matrix notation. For a particular choice of signal parameters A_d, θ_d, A_i, θ_i, τ and T_r, these equations may be solved for W_1 and W_2 and then the behavior of W(t) during the interference repetition period may be found from (19) and (21).

Now consider the initial transient interval again. Suppose the initial weight vector at t=0 is W(0). W(0) could be the steady-state

weight vector with no interference, or could just be an arbitrary initial weight vector. If the weight vector is W(0) when the pulse begins, it will be

$$W_a = e^{-k\Phi_p\tau}[W(0) - \Phi_p^{-1}S\ ] + \Phi_p^{-1}S \tag{24}$$

when the pulse ends. W_a is the initial value for the second transient during the interval $\tau \leq t \leq T_r$ when the pulse is off. At the end of this transient, the weight vector will be W_b:

$$W_b = e^{-k\Phi_o(T_r-\tau)}[W_a - \Phi_o^{-1}S] + \Phi_o^{-1}S. \tag{25}$$

Now consider the quantity $W_b - W_1$. If we substitute (24) for W_a into (25), and substitute (20) for W_2 into (22), and then subtract the second result from the first, we obtain

$$W_b - W_1 = e^{-k\Phi_o(T_r-\tau)-k\Phi_p\tau}[W(0) - W_1]. \tag{26}$$

This result shows how the difference between W(0) and the periodic value W_1 decays in one period. After one period, an initial difference $W(0)-W_1$ has been reduced to $e^{-k\Phi_o(T_r-\tau)-k\Phi_p\tau}[W(0) - W_1]$. To determine how long it takes for the weight vector to settle into a periodic behavior, let M be the matrix

$$M = \Phi_o(T_r-\tau) + \Phi_p\tau. \tag{27}$$

Suppose M has eigenvalues λ'_i and eigenvectors e_i. (M is Hermitian so the λ'_i are real and all three eigenvectors exist.) Using a spectral decomposition formula [10,11], we may write e^{-kM} in the form

$$e^{-kM} = e^{-k\Phi_o(T_r-\tau)-k\Phi_p\tau} = \sum_{i=1}^{3} e^{-k\lambda'_i} e_i e_i^{\dagger}, \tag{28}$$

(where † denotes transpose conjugate), and hence

$$W_b - W_1 = \sum_{i=1}^{3} e^{-k\lambda'_i} e_i e_i^{\dagger} [W(0) - W_1]. \tag{29}$$

From this form it is clear that the decay of $W(0)-W_1$ per pulse repetition period depends on the direction of $W(0)-W_1$ relative to the eigenvectors e_i. Components of $W(0)-W_1$ parallel to eigenvectors associated with large eigenvalues decay rapidly, whereas components parallel to eigenvectors associated with small eigenvalues decay slowly. The duration of the initial transient interval can be calculated in this way. We shall not pursue the initial transient behavior in further detail here. We merely note that it is clear from (26) that the weight vector always approaches a periodic behavior after an initial interval. In the remainder of this paper, we concentrate on the periodic weight behavior and its effect on array performance.

Since pulsed interference causes time-varying weights, such interference causes the response of the array to the desired signal to be time-varying. Thus, the array becomes a time-varying channel. (Such a channel is also called a multiplicative channel or a frequency dispersive channel [12]). For a given weight vector W, the desired signal at the array output is

$$s_d(t) = W^T X_d = A_d W^T U_d e^{j(\omega_o t + \psi_d)}. \tag{30}$$

Since W is time-varying, the output desired signal is modulated. To study this modulation, we define

$$a_d(t) e^{j\eta_d(t)} = A_d W^T U_d. \tag{31}$$

Then $a_d(t) = A_d |W^T U_d|$ is the envelope modulation and $\eta_d = \angle W^T U_d$ is the phase modulation.

The time-varying weights also cause the signal powers at the array output to vary with time. The output desired signal power is

$$P_d = \frac{1}{2} E\left\{ |\tilde{s}_d(t)|^2 \right\} = \frac{1}{2} A_d^2 |W^T U_d|^2, \tag{32}$$

the output interference power is

$$P_i = \begin{cases} \frac{1}{2} A_i^2 |W^T U_d|^2 & : \text{ pulse on} \\ 0 & : \text{ pulse off} \end{cases}, \tag{33}$$

and the output thermal noise power is

$$P_n = \frac{\sigma^2}{2} W^\dagger W. \tag{34}$$

Hence the output interference-to-noise ratio (INR) is

$$\text{Output INR} = \frac{P_i}{P_n} = \begin{cases} \xi_i \dfrac{|W^T U_i|^2}{W^\dagger W} & : \text{ pulse on} \\ 0 & : \text{ pulse off} \end{cases}, \tag{35}$$

and the output signal-to-interference-plus noise ratio (SINR) is

$$\text{SINR} = \frac{P_n}{P_i + P_n} = \begin{cases} \dfrac{\xi_d |W^T U_d|^2}{\xi_i |W^T U_i|^2 + W^\dagger W} & : \text{ pulse on} \\ \dfrac{\xi_d |W^T U_d|^2}{W^\dagger W} & : \text{ pulse off} \end{cases}. \tag{36}$$

In these equations, we use the notation

$$\xi_d = \frac{A_d^2}{\sigma^2} = \text{input SNR per element}, \tag{37}$$

and

$$\xi_i = \frac{A_i^2}{\sigma^2} = \text{input INR per element.} \tag{38}$$

For a given set of signal parameters, (23) can be solved for W_1 and W_2. The weight vector $W(t)$ at a given instant of time may then be computed from (19) for $0 \leq t \leq \tau$ or from (21) for $\tau \leq t \leq T_r$. From $W(t)$, the desired signal modulation and the output INR and SINR may be computed as functions of time using the above formulas.

In carrying out these calculations, it is convenient to use a normalized time variable. In (19), we let

$$e^{-k\Phi_p t} = e^{-\Phi_{pn}(k\sigma^2 t)} = e^{-\Phi_{pn} t'}, \tag{39}$$

where Φ_{pn} is Φ_p normalized to σ^2:

$$\Phi_{pn} = \frac{1}{\sigma^2}\Phi_p = I + \xi_d U_d^* U_d^T + \xi_i U_i^* U_i^T, \tag{40}$$

and where t' is the normalized time variable,

$$t' = k\sigma^2 t. \tag{41}$$

Similarly,

$$e^{-k\Phi_o t} = e^{-\Phi_{on}(k\sigma^2 t)} = e^{-\Phi_{on} t'}, \tag{42}$$

where

$$\Phi_{on} = I + \xi_d U_d^* U_d^T. \tag{43}$$

In Section III, we shall specify the interference signal in terms of its normalized pulse width $\tau' = k\sigma^2\tau$, repetition time $T_r' = k\sigma^2 T_r$ and PRF $f_r' = f_r/k\sigma^2$. (Duty cycle is not affected by this normalization.)

In Section III, we shall also describe the envelope modulation in normalized form. We define the normalized envelope $a_d'(t)$ to be

$$a_d'(t) = \frac{a_d(t)}{A_d|W_o^T U_d|} = \frac{|W^T U_d|}{|W_o^T U_d|} , \tag{44}$$

where $W_o = \Phi_o^{-1} S$. Thus $a_d'(t)$ is the envelope modulation normalized to its value in the absence of interference. Also, because the interference is a periodic waveform, so is $a_d'(t)$. To describe the frequency dispersion of the array, we shall expand $a_d'(t)$ in a Fourier series,

$$a_d'(t) = \sum_{n=-\infty}^{\infty} C_n \, e^{j \frac{2\pi n t}{Tr}} , \tag{45}$$

where the coefficients c_n are given by

$$C_n = \frac{1}{T_r} \int_0^{T_r} a_d'(t) e^{-j\frac{2\pi n t}{T_r}} \, dt, \tag{46}$$

In Section III-F, we present typical frequency spectra of $a_d'(t)$.

Finally, before presenting our results in Section III, we mention that in order to solve (23) for W_1 and W_2, one must calculate the matrices $e^{-\Phi_{pn}\tau'}$ and $e^{-\Phi_{on}(T_r' - \tau')}$. This can be done by means of Sylvester's Theorem [13]. For $e^{-\Phi_{pn}\tau'}$, Sylvester's Theorem is straightforward. One finds

$$e^{-\Phi_{pn}\tau'} = \sum_{i=1}^{3} e^{-\lambda_i \tau'} M_i, \tag{47}$$

where

$$M_i = \prod_{\substack{j=1 \\ j \neq i}}^{3} \frac{(\Phi_{pn} - \lambda_j I)}{(\lambda_i - \lambda_j)} , \tag{48}$$

and where λ_i is the i^{th} eigenvalue of Φ_{pn}. From (40), these eigenvalues are found to be

$$\lambda_1 = 1, \tag{49}$$

and

$$\lambda_{2,3} = 1 + \frac{3}{2}(\varepsilon_d + \varepsilon_i) \pm \frac{1}{2}\sqrt{9(\varepsilon_d - \varepsilon_i)^2 + 4\varepsilon_d\varepsilon_i|U_d^T U_i^*|^2} \tag{50}$$

For $e^{-\Phi_{on}(T_r' - \tau')}$, one must be careful in using Sylvester's Theorem, because Φ_{on} has a repeated eigenvalue*. The expansion for $e^{-\Phi_{on}(T_r' - \tau')}$ contains only two terms:

$$e^{-\Phi_{on}(T_r' - \tau')} = e^{-\lambda_4(T_r' - \tau')} M_4 + e^{-\lambda_5(T_r' - \tau')} M_5, \tag{51}$$

where

$$M_4 = \frac{\Phi_{on} - \lambda_5 I}{\lambda_4 - \lambda_5}, \tag{52}$$

and

$$M_5 = \frac{\Phi_{on} - \lambda_4 I}{\lambda_5 - \lambda_4}. \tag{53}$$

*The expansion of a matrix function with Sylvester's Theorem is usually much more complicated when the matrix has repeated eigenvalues [14] than when all its eigenvalues are distinct [15]. However, a Hermitian matrix has a full set of eigenvectors, even if it has repeated eigenvalues. For this reason, Sylvester's Theorem for such a matrix can be derived using the simple method given by Hildebrand [15] except that with repeated eigenvalues one must start with the reduced characteristic equation [16] instead of the full Cayley-Hamilton Theorem [16]. Sylvester's Theorem for a Hermitian matrix with repeated eigenvalues contains fewer terms than with distinct eigenvalues, because there is only one term in the expansion for each repeated eigenvalue.

λ_4 and λ_5 are the two distinct eigenvalues of Φ_{on}, given by

$$\lambda_4 = 1, \tag{54}$$

and

$$\lambda_5 = 1 + 3\varepsilon_d. \tag{55}$$

(Φ_{on} has two eigenvalues equal to 1.)

With this background, we now discuss the numerical results obtained from these equations.

III. RESULTS

In this section we describe the performance of the array in the presence of pulsed interference. In Part A, we show typical curves of desired signal modulation, output INR and SINR as functions of time. Parts B-E show how the signal parameters affect desired signal modulation. In Part F, we show typical output desired signal spectra, to illustrate the frequency dispersion of the array. Finally, in Part G we assume the array is used in a digital communication system and show how pulsed interference affects bit error probability.

A. Typical Waveforms

First, we show typical curves of desired signal modulation, output INR and SINR as functions of time.

We begin with the envelope modulation. Figure 3 shows the desired signal envelope modulation for $\Theta_d = 0^\circ$, $\Theta_i = 5^\circ$, $\xi_d = 10$ dB, $\xi_i = 20$ dB, $\delta = .1$ and $f_r' = 1$. The graph shows $a_d'(t')$ versus t' over one period of the modulation, $0 \leq t' \leq T_r'$. This is a typical curve, and it is seen that the interference produces substantial envelope modulation.

Next, we consider the phase modulation. When $\eta_d(t)$ is calculated, one discovers an interesting result: pulsed interference does not produce any phase modulation, regardless of the signal parameters. This result occurs because with pulsed interference, the weight vector moves back and forth between two values, $\Phi_o^{-1}S$ and $\Phi_p^{-1}S$. It can be shown that when the weight vector is equal to either of these values, the desired signal at the array output is matched in phase to the reference signal. In addition, it turns out that during an exponential transient from one of these values to the other, as in (19) or (21), the desired signal phase at the array output remains fixed for all t'. (This statement can be proven analytically, but the details are tedious and we omit them here.) As a result, there is no phase modulation, regardless of the signal parameters A_d, Θ_d, A_i, Θ_i, τ or T_r.

It should be pointed out that $\eta_d(t)$ is zero only <u>after</u> the array weights are periodic. Phase modulation <u>can</u> occur during an initial weight transient before the weights have become periodic. The amount of phase modulation during an initial transient depends on the initial weight vector

when the interference first appears. If the array weights are initially aligned on the desired signal (i.e., if $W(0) = \Phi_o^{-1}S$), there will be no phase modulation during the initial transient. But if the initial weight vector is such that the desired signal at the array output is not in phase with the reference signal, phase modulation will occur. However, once the initial transient period is over, there is no further phase modulation.

Next, we consider the output INR and SINR. Figures 4 and 5 show the output INR and SINR for the same conditions as in Figure 3. Each quantity is shown as a function of time over one period of the interference. Figure 4 shows the interference pulse as it appears at the array output. Since the array is nulling the interference, the output INR drops during the pulse. The SINR in Figure 5 has the corresponding behavior. When the interference disappears at the end of the pulse, the SINR jumps up.

These first curves are intended merely to illustrate typical array behavior. In Parts B-F below, we examine in detail the effect of each signal parameter on the desired signal modulation. Also, to evaluate the significance of the time-varying SINR, in Part G we assume the desired signal is a digital communication signal and compute the effect of the SINR on the bit error probability.

In order to describe the modulation effects in Parts B-E, we now define certain quantities that will be useful to characterize the modulation. First we define a_{max} to be the largest and a_{min} the smallest value of $a_d'(t')$ during the pulse repetition period. Then we also define

$$m = \frac{a_{max} - a_{min}}{a_{max}} . \tag{56}$$

In the sequel, we examine how a_{max} and m depend on the signal parameters. a_{max} is a useful quantity to study because it measures how much the desired signal is suppressed at the peak of its envelope. With no interference, a_{max} is unity. With interference, a_{max} drops below unity. We shall refer to a_{max} as the envelope peak. m is of interest because it measures the amount of envelope modulation. Since m is the peak-to-peak envelope variation normalized to the peak, it may be thought of as "fractional" modulation, analogous to percentage modulation in classical AM. We shall refer to m as the envelope variation.

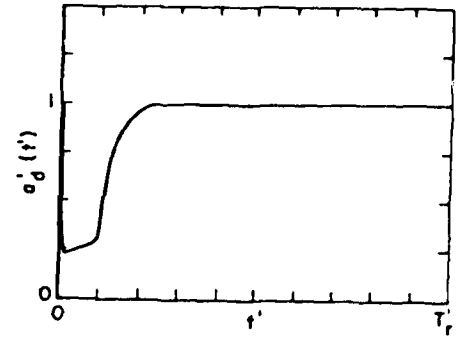

Figure 3. Desired Signal Amplitude vs. Time
$\theta_d=0^0$, $\theta_i=5^0$, SNR=10 dB, INR=20 dB, $f_r' = 1$, $\delta=0.1$

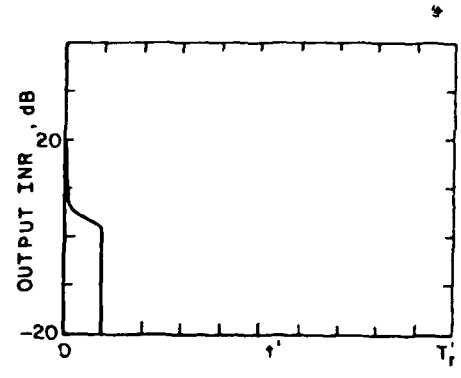

Figure 4. Output INR vs. Time
$\theta_d=0^0$, $\theta_i=5^0$, SNR=10 dB, INR=20 dB, $f_r' = 1$, $\delta=0.1$

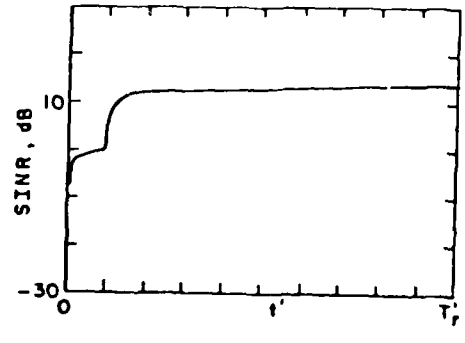

Figure 5. Output SINR vs. Time
$\theta_d=0^0$, $\theta_i=5^0$, SNR=10 dB, INR=20 dB, $f_r'=1$, $\delta=0.1$

In the computer programs used to obtain the data below, a_{max} and a_{min} have been computed as follows. The envelope peak always occurs at the beginning of the pulse (as in Figure 3). Hence a_{max} is equal to $|W_1^T U_d|/|W_o^T U_d|$. The minimum envelope, on the other hand, can occur at different times. In some cases a_{min} occurs during the pulse, and in others at the end of the pulse. (Figure 3 shows a case where a_{min} occurs during the pulse). To obtain the data below, a_{min} has been found by searching the interval $0 \leq t \leq \tau$ for the smallest value of the envelope.

Using several computer programs, we have explored the behavior of the peak a_{max} and the variation m as functions of the signal parameters. In the following sections we summarize these results.

B. The Effect of Angle of Arrival

Desired signal modulation effects are large only when Θ_i is close to Θ_d. When Θ_i is far from Θ_d, the variation m is small and the peak a_{max} is large*.

Figure 6 shows a typical result; it shows m as a function of Θ_i when $\Theta_d=0^o$ and for $f_r'=1$, $\delta=.01$ and $\xi_d=6$ dB. Four different curves are shown, for INR = 0, 10, 20, and 30 dB. It is seen that large values of m occur only when $\Theta_i \approx \Theta_d$. One finds that this conclusion holds true regardless of the particular Θ_d. (Note that Figure 3, which shows a case with large modulation, is for $\Theta_d = 0^o$, $\Theta_i = 5^o$).

m is small unless $\Theta_i \approx \Theta_d$ for the following reason. With pulsed interference, the weight vector swings back and forth between $\Phi_o^{-1}S$ and $\Phi_p^{-1}S$. A large modulation is produced only if the desired signal response with weight vector $\Phi_p^{-1}S$ is substantially different from that with $\Phi_o^{-1}S$. It turns out that these two responses are different only when the interference signal is near the desired signal. To illustrate this, let a_o be the desired signal response of the array with $W = \Phi_o^{-1}S$ and a_p be

*An exception to this occurs if the interference causes a grating null in the desired signal direction. In the discussion here, it is assumed that the element patterns and spacings have been chosen to avoid grating nulls [17].

the response with $W = \Phi_p^{-1}S$ (i.e., with CW interference). Figure 7 shows a plot of a_p/a_o as a function of θ_i under the same conditions as in Figure 6 ($\theta_d = 0^o$ and $\xi_d = 6$ dB). As may be seen, desired signal suppression with CW interference is large only if the interference is close to the desired signal.

Figure 8 shows the peak a_{max} as a function of θ_i for $\theta_d = 0^o$, $\xi_d = 6$ dB, $f_r' = 1000$ and $\delta = .1$. (The values of f_r' and δ used here differ from those in Figure 6. The reason for these choices will be clear after the effects of f_r' and δ on signal modulation have been discussed below). Figure 8 shows that a_{max} differs from unity only when $\theta_i \approx \theta_d$. I.e., the interference must be close to the desired signal to cause a large suppression of the peak. This result occurs for the same reason discussed above. The desired signal response with weight vector $\Phi_p^{-1}S$ must be smaller than with weight vector $\Phi_o^{-1}S$ for the interference to suppress the peak.

In essence, modulation effects are large only if the interference and desired signals are too close for the array to resolve. However, it should be noted that continuous interference also causes difficulty in this case. With continuous interference, there is no modulation, of course, but the SINR drops as θ_i approaches θ_d.

C. The Effect of PRF

The variation m and peak a_{max} are large at low PRF and drop as the PRF increases.

Consider the case where the pulse width is fixed. (The effect of pulse width is discussed in Part D). Figures 9 and 10 show m and a_{max} as functions of f_r' for $\xi_d = 6$ dB, $\xi_i = 40$ dB, $\theta_d = 0^o$ and $\tau' = .0001$. Several curves are shown in each figure for different θ_i near θ_d. It is seen that m and a_{max} are large for small f_r' and drop as f_r' becomes large. (Also, note that m decreases and a_{max} increases as θ_i gets farther from θ_d, as discussed in Part B).

This behavior occurs for the following reason. The value of τ' used in Figures 9 and 10 is large enough that there is sufficient time during the pulse for the weights to change substantially in response to the interference. At low PRF, there is also enough time between pulses for the weights to return to the values they would have no interference. But

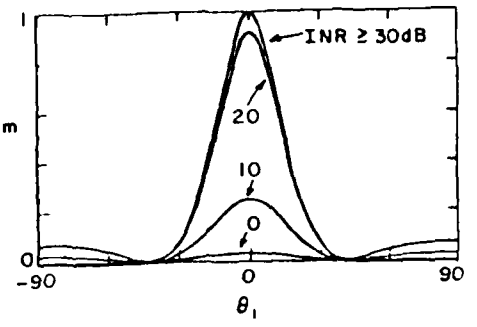

Figure 6. Envelope Variation m vs. Θ_j
$\Theta_d=0^0$, f_r = 1, SNR=6 dB, δ=0.01

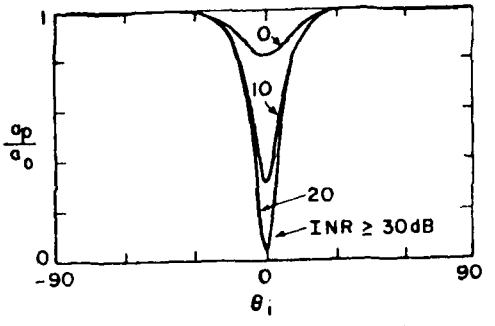

Figure 7. Desired Signal Attenuation vs. Θ_j for CW Interference
$\Theta_d=0^0$, SNR=6 dB

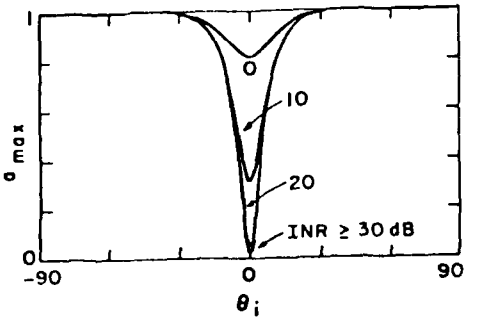

Figure 8. Envelope Peak a_{max} vs. Θ_j
$\Theta_d=0^0$, f_r'=1000, SNR=6 dB, δ=0.1

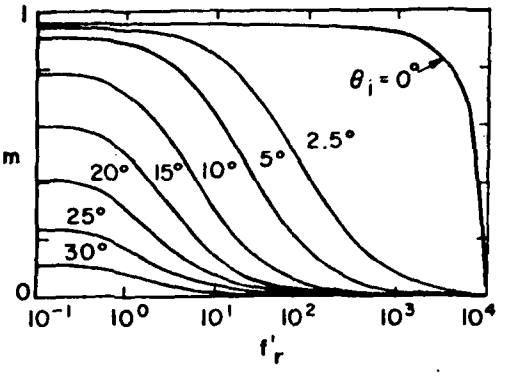

Figure 9. Envelope Variation vs. PRF
SNR=6 dB, INR=40 dB, $\theta_d=0^0$, $\tau'=.0001$

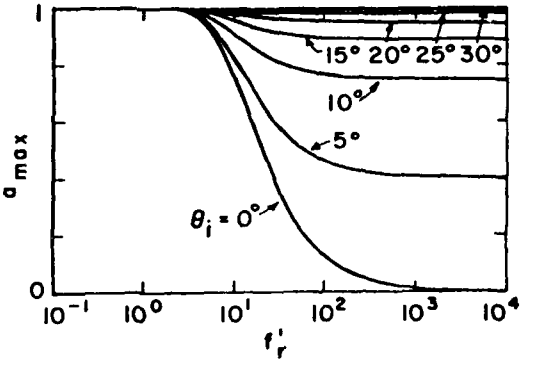

Figure 10. Envelope Peak vs. PRF
SNR=6 dB, INR=40 dB, $\theta_d=0^0$, $\tau'=.0001$

at high PRF, the weights do not have time to recover from the interference, so the variation is reduced and the peak drops.

If m and a_{max} are computed versus f_r' with the duty cycle held constant instead of the pulse width, the same conclusion still holds: m and a_{max} are large for small f_r' and drop as f_r' increases. Curves of m and a_{max} versus f_r' for fixed δ are presented below in Part D. (Figures 17-22).

D. The Effect of Pulse Width and Duty Cycle

The longer the pulse width, the more quickly m and a_{max} change with f_r'.

Figures 11-16 illustrate this behavior. Figures 11-13 show m versus f_r', as in Figure 9, but with $\tau' = .001$, .01 and .1. (When $f_r' = 1/\tau'$, the interference is actually CW, so the curves stop at this value of f_r'). Note that as τ' becomes larger, m drops more quickly as a function of f_r'. Figures 14-16 show a_{max} as a function of f_r' for the same values of τ'. (Compare these curves with Figure 10 for $\tau' = .0001$). Again, the range of f_r' over which a_{max} changes becomes smaller as τ' increases.

The reason for this behavior is as follows. For low values of f_r', τ' has little effect on the time between pulses. But as τ' is made larger, the time between pulses drops more quickly as f_r' is increased. As the time between pulses drops, so do m and a_{max}, because when this time is too short the array cannot recover between pulses.

Figures 11-16 have been computed for constant pulse width. It is also interesting to examine m and a_{max} as functions of f_r' for constant duty cycle, instead of pulse width. Figures 17-19 show m versus f_r' with $\delta = .0001$, .001 and .01, and Figures 20-22 show a_{max} versus f_r' for the same δ's. Comparing Figures 17-19 shows that as δ is raised, m remains large up to higher values of f_r'. Figures 20-22 show, however, that the value of f_r' at which a_{max} begins to drop below unity is not affected by δ. (a_{max} begins to decrease around $f_r' = 3$, regardless of δ). Increasing δ merely causes the smallest value of a_{max} (at high f_r') to decrease.

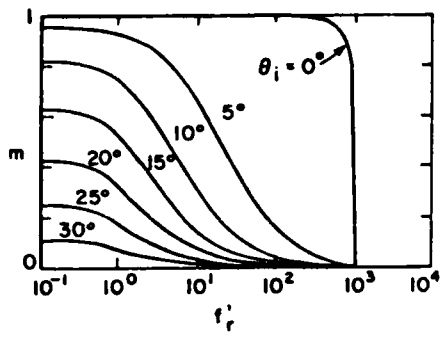

Figure 11. Envelope Variation vs. PRF
$\theta_d=0^0$, SNR=6 dB, INR=40 dB, $\tau'=.001$

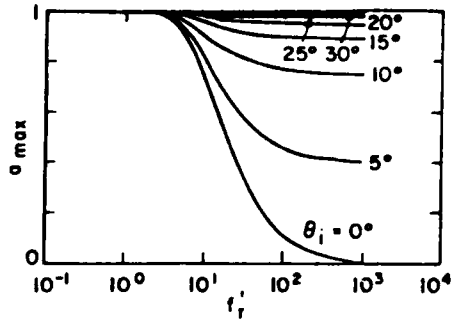

Figure 14. Envelope Peak vs. PRF
$\theta_d=0^0$, SNR=6 dB, INR=40 dB, $\tau'=.001$

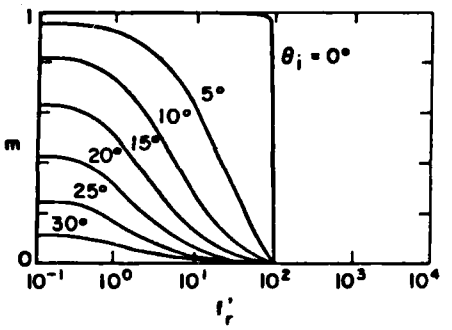

Figure 12. Envelope Variation vs. PRF
$\theta_d=0^0$, SNR=6 dB, INR=40 dB, $\tau'=.01$

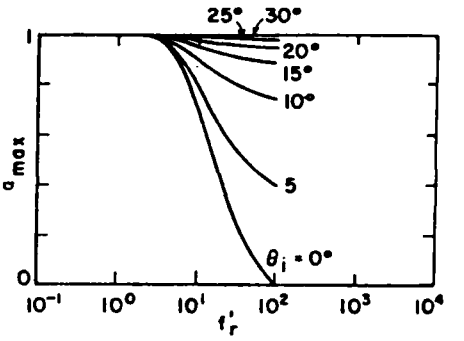

Figure 15. Envelope Peak vs. PRF
$\theta_d=0^0$, SNR=6 dB, INR=40 dB, $\tau'=.01$

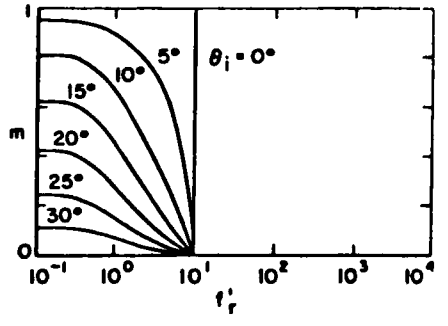

Figure 13. Envelope Variation vs. PRF
$\theta_d=0^0$, SNR=6 dB, INR=40 dB, $\tau'=.1$

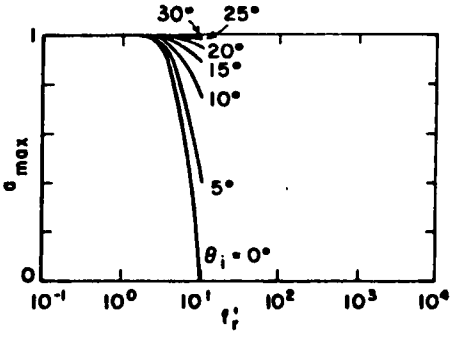

Figure 16. Envelope Peak vs. PRF
$\theta_d=0^0$, SNR=6 dB, INR=40 dB, $\tau'=.1$

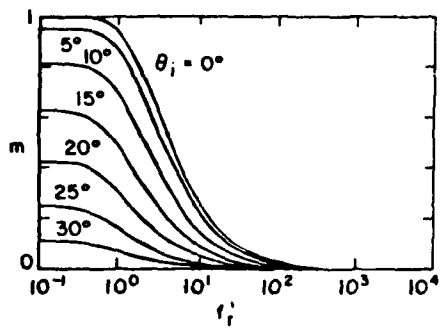

Figure 17. Envelope Variation vs. PRF
$\theta_d=0^0$, SNR=6 dB, INR=40 dB, δ=.0001

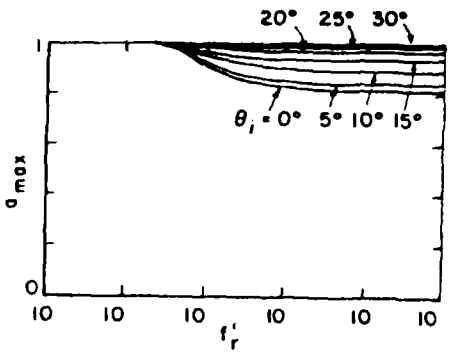

Figure 20. Envelope Peak vs. PRF
$\theta_d=0^0$, SNR= 6 dB, INR=40 dB, δ=.0001

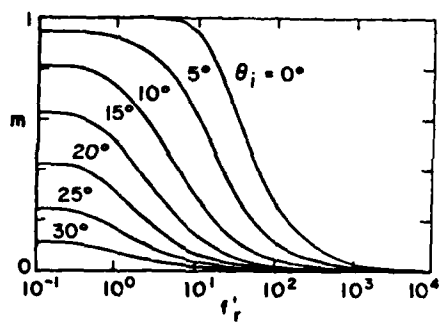

Figure 18. Envelope Variation vs. PRF
$\theta_d=0^0$, SNR=6 dB, INR=40 dB, δ=.001

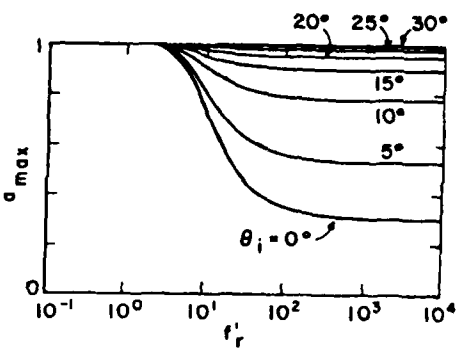

Figure 21. Envelope Peak vs. PRF
$\theta_d=0^0$, SNR=6 dB, INR=40 dB, δ=.001

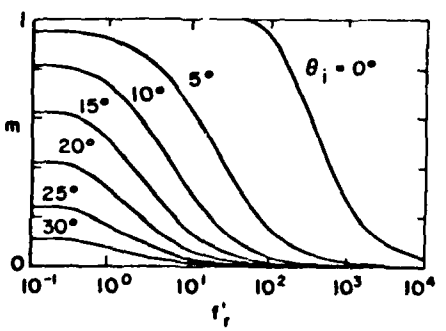

Figure 19. Envelope Variation vs. PRF
$\theta_d=0^0$, SNR=6 dB, INR=40 dB, δ=.01

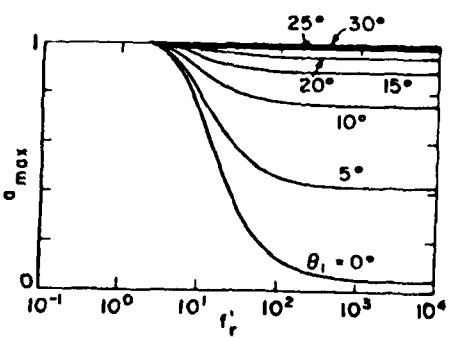

Figure 22. Envelope Peak vs. PRF
$\theta_d=0^0$, SNR=6 dB, INR=40 dB, δ=.01

E. The Effect of Signal-to-Noise Ratios

m is largest and a_{max} is smallest for low SNR and high INR. As the SNR is increased or the INR is decreased, m decreases and a_{max} increases.

Figures 23-26 illustrate these remarks. Figure 23 shows m versus f_r', for $\tau' = .0001$, $\theta_d = 0^0$, $\theta_i = 10^0$ and INR = 40 dB. Curves are shown for several SNR's between 20 and 50 dB. Figure 24 shows m versus f_r' for SNR=10 dB and for several INR's between 20 and 45 dB. As may be seen, m is maximum for low SNR and high INR and decreases as the SNR increases or the INR decreases. Figure 25 shows a_{max} versus f_r' for INR=40 dB and for -10 dB $\leq$ SNR $\leq$ 20 dB, and Figure 26 shows a_{max} versus f_r' for SNR=0 dB and -10 dB $\leq$ INR $\leq$ 40 dB. We see how the lowest value of a_{max} (at large f_r') increases as the SNR increases. Decreasing the INR moves the curves of a_{max} versus f_r' farther to the right. For a given f_r', the result is that decreasing the INR will increase a_{max}.

F. Frequency Dispersion

Next we consider the frequency dispersion of the array with pulsed interference. As we have seen, pulsed interference results in a periodic envelope modulation of the output desired signal. Hence the output desired signal has a line spectrum with harmonics at multiples of the pulse repetition frequency. We may determine the frequency dispersion of the array by computing the Fourier coefficients C_n in (46) as a function of the signal parameters.

Unfortunately, space does not allow us to show an exhaustive set of spectra here. Instead, we shall content ourselves with a few typical results.

First, Figure 27 illustrates the effect of pulse width on the spectrum. These spectra are for $\theta_d = 0^0$, $\theta_i = 5^0$, SNR=0 dB, INR=30 dB and $f_r' = 1$. Spectra are shown for several values of τ' between .00001 and .05. The plots show $|C_n|$ in dB ($20 \log_{10}|C_n|$) plotted versus frequency over the frequency range $f_o' - 125 \leq f' \leq f_o' + 125$, where f_o' is (normalized) carrier frequency. Thus, the curves show 125 harmonics on either side of the carrier. It may be seen that with $\tau' = .00001$ there is almost no frequency dispersion, but as τ' is increased the spectrum covers a wider frequency range and becomes more complicated.

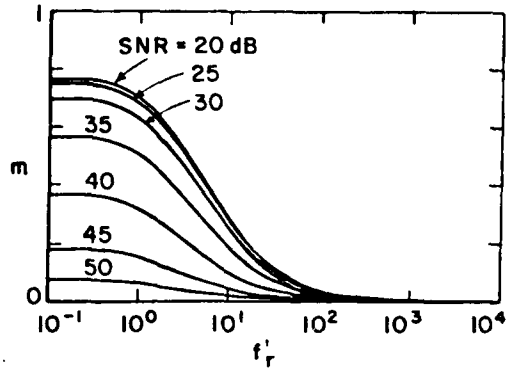

Figure 23. Envelope Variation vs. PRF
θ_d=0°, θ_i=10°, INR=40 dB, τ'=.0001

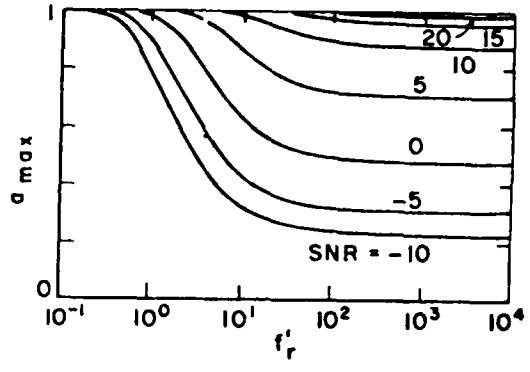

Figure 25. Envelope Peak vs. PRF
θ_d=0°, θ_i=10°, INR=40 dB, τ'=.0001

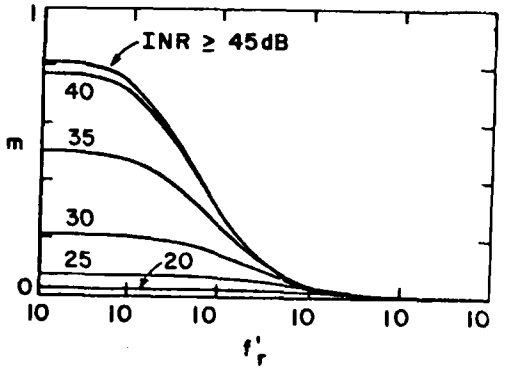

Figure 24. Envelope Variation vs. PRF
θ_d=0°, θ_i=10°, SNR=10 dB, τ'=.0001

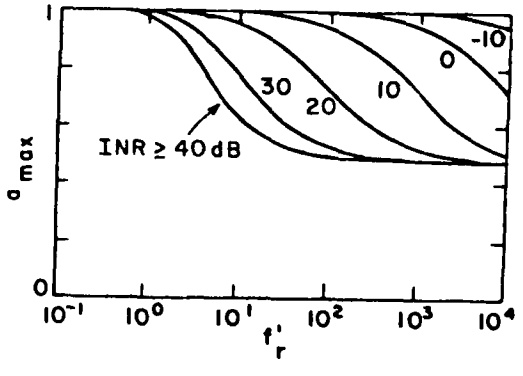

Figure 26. Envelope Peak vs. PRF
θ_d=0°, θ_i=10°, SNR=0 dB, τ'=.0001

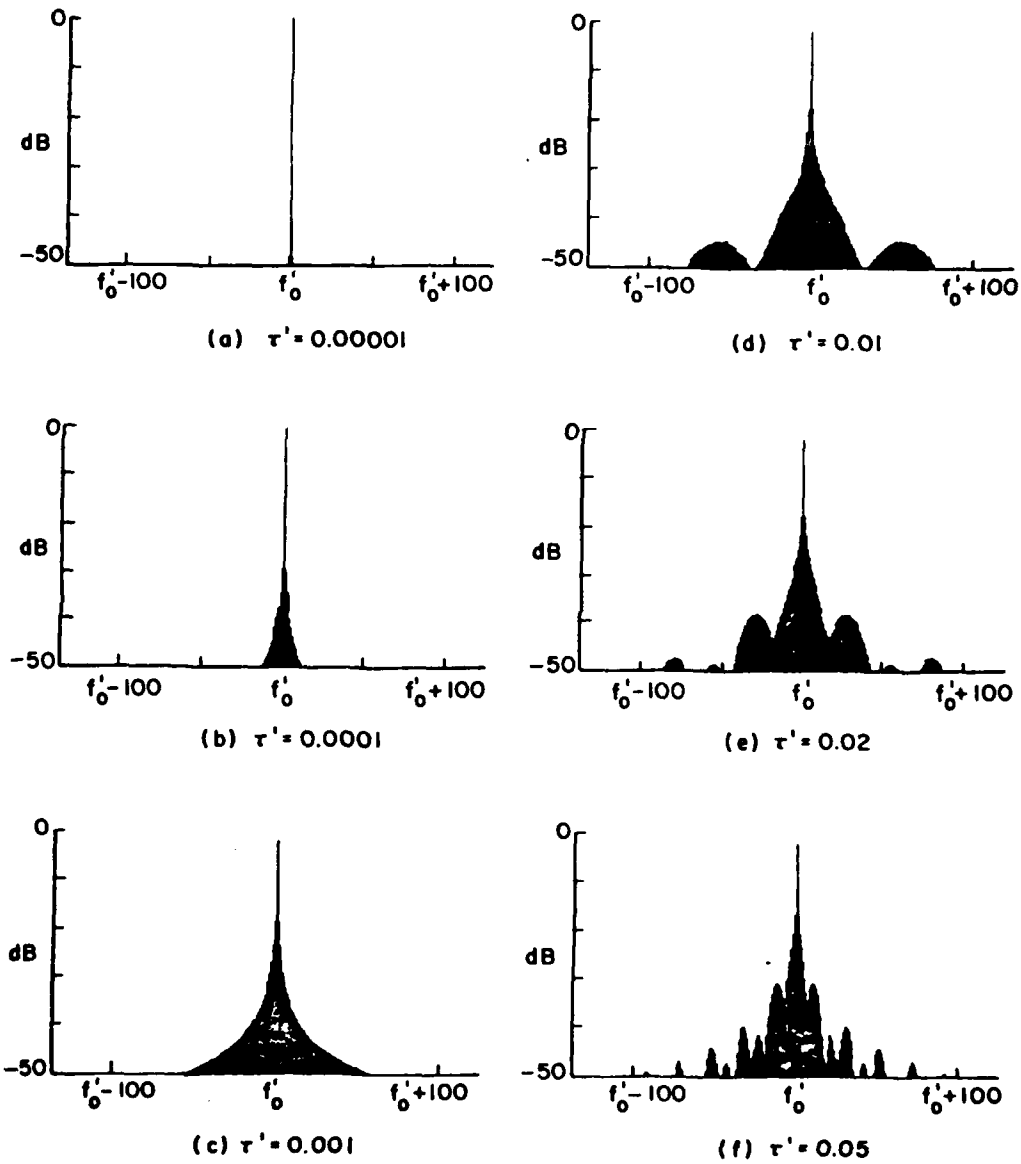

Figure 27. Desired Signal Power Spectrum
$\theta_d=0^0$, $\theta_1=5^0$, SNR=0 dB, INR=30 dB, $f_r'=1$

Next, Figure 28 shows spectra illustrating the effect of changing the pulse repetition frequency. These plots show $|C_n|$ versus frequency for the same conditions as in Figure 27 except now $\tau' = .001$ and f_r' is varied. Spectra are shown for four different f_r': 10, 50, 100 and 500, and are plotted over the frequency range $f_o' - 12500 \leq f' \leq f_o' + 12500$. Note how the bandwidth of the modulation changes with f_r'.

In general, many different spectral patterns may be obtained as the signal parameters are varied. If f_r' is large, the spectrum may extend very far from the carrier. However, the overall bandwidth does not exceed a value determined by the signal powers. That is, the powers control the eigenvalues of Φ and hence the speed of the array weights. The spectrum always tapers off beyond the frequency range where the weights are too slow to respond.

G. Bit Error Probability

Finally, in this last part, we evaluate the effect of the time-varying SINR discussed in Part A by computing its effect on bit error probability when the desired signal is a digital communication signal.

To have a specific case to consider, we arbitrarily assume the desired signal is a differential phase shift keyed (DPSK) signal of the form [18]

$$\tilde{s}(t) = A_d e^{j[\omega_o t + \psi_d + \alpha_d(t)]} , \qquad (57)$$

where $\alpha_d(t)$ is 0 or π on each bit interval of length T_b. $\alpha_d(t)$ is obtained by differentially encoding the source bits [18]. We again assume that the reference signal is a replica of the desired signal.

Before discussing the bit error probability, we point out that changing the desired signal to a biphase modulated signal, instead of a CW signal, will have no effect on the array weights. As long as the bandwidth is not excessive, the covariance matrix Φ is the same as for a CW signal. (Also, it has been shown [19] that desired signal bandwidth has almost no effect on array performance anyway, even if the bandwidth is large). Moreover, if the reference signal is replica of the desired

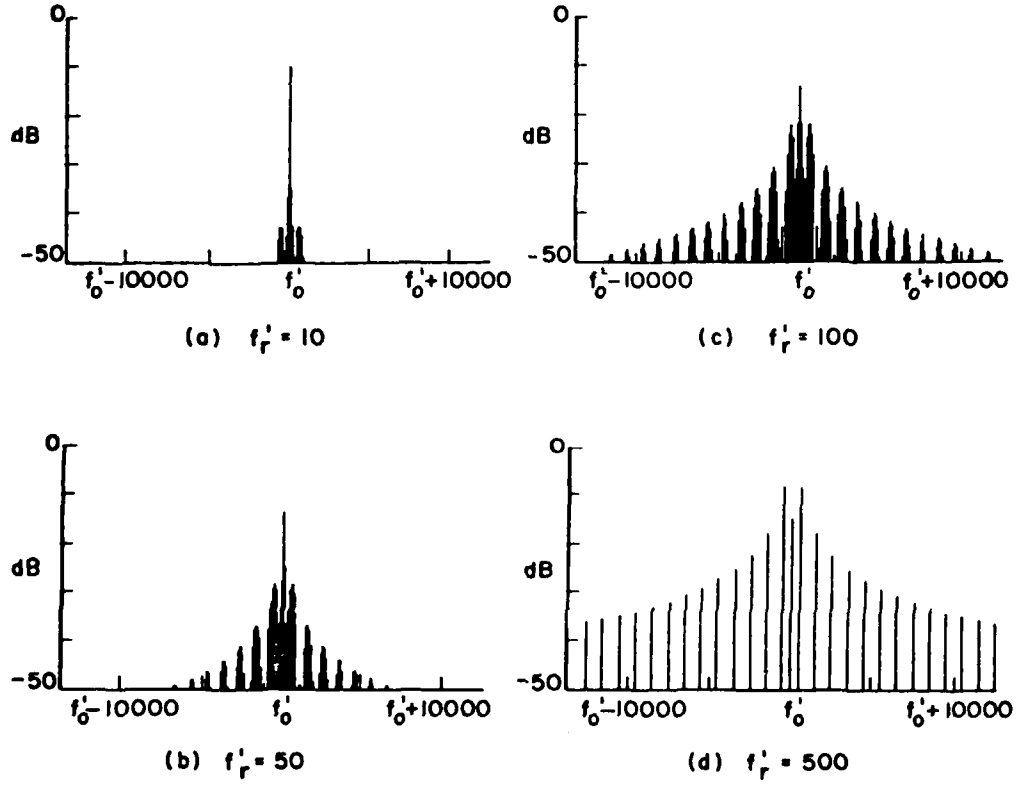

Figure 28. Desired Signal Power Spectrum
$\theta_d=0^0$, $\theta_1=5^0$, SNR=0 dB, INR=30 dB, τ'=.001

signal, the reference correlation vector S is also unchanged. Since both Φ and S are the same, the weight behavior will be the same with this signal as with the CW signal.

Because pulsed interference does not produce phase modulation on the desired signal, the only effect of the interference on system performance will be to vary the array output SINR and hence increase the bit error probability. For a DPSK signal in white noise, the bit error probability p_e is given by [20]:

$$P_e = \frac{1}{2} e^{-E_b/N_o} , \tag{58}$$

where E_b is the signal energy per bit and N_o is the one-sided thermal noise spectral density. For our purposes, it is convenient to express E_b/N_o in terms of signal-to-noise ratio. Since $E_b = P_d T_b$, where P_d is signal power and T_b is the bit duration, and since $1/T_b$ is the effective noise bandwidth, N_o/T_b is the received noise power and we may write

$$\frac{E_b}{N_o} = \frac{P_d}{(N_o/T_b)} = SNR. \tag{59}$$

In addition, for this analysis we shall assume the interference power at the array output has the same effect on detector performance as thermal noise power. In this case, the bit error probability may be written

$$P_e = \frac{1}{2} e^{-SINR} . \tag{60}$$

Finally, since pulsed interference causes the SINR to vary periodically, we obtain the effective bit error probability $\overline{P}_e$ by averaging P_e over one period of the interference:

$$\overline{P}_e = \frac{1}{T_r} \int_0^{T_r} \frac{1}{2} e^{-SINR(t)} \, dt. \tag{61}$$

This calculation is valid as long as the bit rate is large compared with the interference PRF, which we assume to be the case.

Figure 29 shows typical curves of bit error probability computed in this manner. These curves show $\bar{P}_e$ as a function of PRF for $\theta_d = 0^o$, $\theta_i = 30^o$, SNR = 6 dB, $\tau' = .0001$ and for four INR's: 10, 20, 30 and 40 dB. It is interesting to note that intermediate values of f_r' produce the greatest $\bar{P}_e$. For low or high f_r', the interference has less effect.* Also, values of INR less than 10 dB or greater than 40 dB produce lower values of $\bar{P}_e$ than those shown in Figure 29.

The curves in Figure 29 are for $\theta_d = 0^o$ and $\theta_i = 30^o$, i.e., for a large angular separation between signals. As θ_i is brought closer to θ_d, both the peak $\bar{P}_e$ and value of f_r' at the peak rise. Increasing the separation between θ_i and θ_d does not change the results much, however. The curves in Figure 29 are typical of what is obtained when the two signals are far enough apart to be resolved by the array.

It is also interesting to see how the other signal parameters affect the value of f_r' at the peak $\bar{P}_e$. As may be seen in Figure 29, the value of f_r' at the peak depends somewhat on the INR. The higher the INR, the lower the f_r'. It turns out that the SNR and the pulse width also have some effect on the value of f_r' at peak $\bar{P}_e$. As the SNR or the pulse width increase, the value of f_r' at the peak drops.

---

*Similar results have been obtained by Reinhard, based on experimental measurements [21].

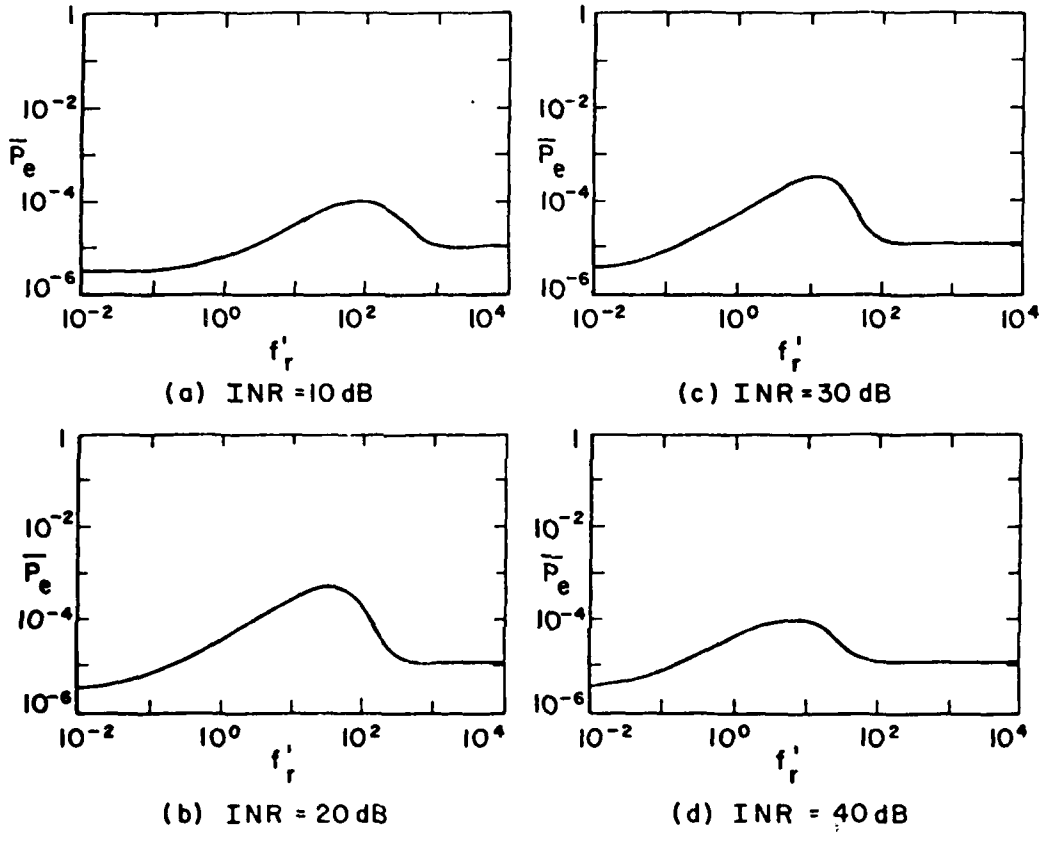

Figure 29. Bit Error Probability vs. PRF.
SNR=6 dB, $\theta_d=0^0$, $\theta_i=30^0$, $\tau'=.0001$

IV. CONCLUSIONS

Pulsed interference has two effects on an adaptive array receiving a desired signal. First, it produces envelope modulation of the desired signal and second, it causes the array output SINR to vary. When the array is used in a digital communication system, this varying SINR results in an increased bit error probability.

The desired signal modulation depends on the signal parameters as follows:

(1) The envelope variation is small and the envelope peak is large unless the interference angle is close to the desired signal angle.

(2) The envelope variation and peak are both largest at low interference PRF and drop as the PRF increases.

(3) The envelope variation and peak change more quickly with PRF as the pulse width is increased.

(4) The envelope variation is largest for low SNR and high INR. The envelope peak is largest for high SNR and low INR.

(5) Pulsed interference does not produce phase modulation on the desired signal after the initial transient.

Since the array modulates the desired signal, the array becomes a frequency dispersive channel. Typical frequency spectra of the array output desired signal were shown in Figures 27 and 28.

Pulsed interference causes the array output SINR to vary with time. When the array is used in a digital communication system, the result is to increase the bit error probability. The largest bit error probability occurs for intermediate values of interference PRF. Typical curves are shown in Figure 29.

REFERENCES

1. B. Widrow, P.E. Mantey, L.J. Griffiths and B.B. Goode, "Adaptive Antenna Systems," Proc. IEEE, vol. 55, p. 2143, Dec. 1967.

2. W.F. Gabriel, "Adaptive Arrays - An Introduction," Proc. IEEE, vol. 64, p. 239, Feb. 1976.

3. R.L. Riegler and R.T. Compton, Jr., "An Adaptive Array for Interference Rejection," Proc. IEEE, vol. 61, p. 748, June 1973.

4. R.T. Compton, Jr., R.J. Huff, W.G. Swarner and A.A. Ksienski, "Adaptive Arrays for Communication Systems: An Overview of Research at The Ohio State University," IEEE Trans. Antennas and Propagation, vol. AP-24, p. 599, Sept. 1976.

5. R.T. Compton, Jr., "An Adaptive Array in a Spread Spectrum Communication System," Proc. IEEE, vol. 66, p. 289, March, 1978.

6. R.T. Compton, Jr., "On the Performance of a Polarization Sensitive Adaptive Array," to appear in IEEE Trans. Antennas and Propagation.

7. R.T. Compton, Jr., "The Tripole Antenna - An Adaptive Array with Full Polarization Flexibility," to appear in IEEE Trans. Antennas and Propagation.

8. M. Athans, M.L. Dertouzos, R.N. Spann and S.J. Mason, Systems, Networks and Computation, McGraw-Hill Book Co., New York, 1974.

9. R. Bellman, Introduction to Matrix Analysis, McGraw-Hill Book Co., New York, 1970.

10. B. Friedman, Principles and Techniques of Applied Mathematics, John Wiley and Sons, Inc., New York, 1956.

11. P.R. Halmos, Finite-Dimensional Vector Spaces, D. Van Nostrand Co., Inc., Princeton, N.J., 1958.

12. R.S. Kennedy, Fading, Dispersive, Communication Channels, John Wiley and Sons, Inc., New York, 1969.

13. F.B. Hildebrand, Methods of Applied Mathematics, Prentice-Hall, Inc., Englewood Cliffs, N.J., 1952.

14. R.A. Frazer, W.J. Duncan and A.R. Collar, Elementary Matrices, Cambridge University Press, London, 1946.

15. Hildebrand, op. cit., p. 65-66.

16. Ibid., p. 64.

17. A. Ishide and R.T. Compton, Jr., "On Grating Nulls in Adaptive Arrays," IEEE Trans. Antennas and Propagation, vol. AP-28, p. 467, July 1980.

18. R.E. Ziemer and W.H. Tranter, Principles of Communications, Houghton Mifflin Co., Boston, 1976.

19. W.E. Rodgers and R.T. Compton, Jr., "Adaptive Array Bandwidth with Tapped Delay-Line Processing," IEEE Trans. Aerospace and Electronic Systems, vol. AES-15, p. 21, January 1979.

20. W.C. Lindsey and M.K. Simon, Telecommunication Systems Engineering, Prentice-Hall Inc., Englewood Cliffs, N.J., 1973.

21. K.L. Reinhard, "Adaptive Antenna Arrays for Coded Communication Systems," Ph.D. dissertation, Department of Electrical Engineering, Ohio State University, Columbus, Ohio, October 1973.